

Applications of Skyrme energy-density functional to fusion reactions spanning the fusion barriers

Min Liu^a, Ning Wang^{b,*}, Zhuxia Li^{a,b,c}, Xizhen Wu^{a,c}, Enguang Zhao^{b,d}

^a *China Institute of Atomic Energy, Beijing 102413, PR China*

^b *Institute of Theoretical Physics, Chinese Academic of Science, Beijing 100080, PR China*

^c *Nuclear Theory Center of National Laboratory of Heavy Ion Accelerator, Lanzhou 730000, PR China*

^d *Department of Physics, Tsinghua University, Beijing 100084, PR China*

Received 18 April 2005; received in revised form 20 December 2005; accepted 20 January 2006

Available online 3 February 2006

Abstract

The Skyrme energy density functional has been applied to the study of heavy-ion fusion reactions. The barriers for fusion reactions are calculated by the Skyrme energy density functional with proton and neutron density distributions determined by using restricted density variational (RDV) method within the same energy density functional together with semi-classical approach known as the extended semi-classical Thomas–Fermi method. Based on the fusion barrier obtained, we propose a parametrization of the empirical barrier distribution to take into account the multi-dimensional character of real barrier and then apply it to calculate the fusion excitation functions in terms of barrier penetration concept. A large number of measured fusion excitation functions spanning the fusion barriers can be reproduced well. The competition between suppression and enhancement effects on sub-barrier fusion caused by neutron-shell-closure and excess neutron effects is studied.

© 2006 Elsevier B.V. All rights reserved.

1. Introduction

A large number of fusion excitation functions have been accumulated in recent decades [1–3], which provides a possibility for a systematic study on fusion reactions. Newton et al. [4] analyzed a total of 46 fusion excitation functions at energies above the average fusion barriers

* Corresponding author.

E-mail addresses: ning.wang@theo.physik.uni-giessen.de (N. Wang), lizwux@iris.ciae.ac.cn (Z. Li).

using the Woods–Saxon form for the nuclear potential in a barrier passing model of fusion. They found that the empirical diffuseness parameters a ranging between 0.75 and 1.5 were considerably larger than those obtained from elastic scattering data and the deduced a showed strong increase with increasing the charge product $Z_1 Z_2$. Thus, it results in a certain difficulty for giving satisfied predictions of fusion cross sections for unmeasured reaction systems. The fusion coupled channel model is successful for describing fusion excitation function of heavy-ion reaction at energies near fusion barrier. However, with the increasing of the neutron excess and the charges (the product $Z_1 Z_2$) of two nuclei, the fusion coupled channel model encounters a lot of difficulties due to a very large number of degrees of freedom involved. In order to carry out a systematic study of fusion excitation functions, a simple and useful approach seems to be required. A semi-empirical approach in which the quantum penetrability of Coulomb barrier is calculated by using the concept of barrier distribution arising due to the multi-dimensional character of the real nucleus–nucleus interaction [5–7] is very helpful in this aspect. Thus, a reasonable parametrization of the weighing function describing the barrier distribution based on the interaction potential in the entrance channel seems to be very useful.

In [8] the interaction potential in the entrance channel for fusion reactions was calculated based on the semi-classical expressions of the Skyrme energy density functional [9–11]. In the calculation of the interaction potential, which is the difference between the energy of the total system and the energies of individual projectile and target, the density distributions of the projectile and target are required. In [8] the density distributions of the projectile and target were determined by Hartree–Fock–Bogoliubov calculations. According to the Hohenberg and Kohn theorem [12], the energy of a N -body system of interaction fermions is a unique functional of local density. In the framework of the semi-classical extended Thomas–Fermi (ETF) approach together with a Skyrme effective nuclear interaction such a functional can be derived systematically. The density functional theory is widely used in the study of the nuclear ground state which provides us with a useful balance between accuracy and computation cost allowing large systems with a simple self-consistent manner. Thus, it is very suitable to perform the calculation of the entrance-channel potential and the densities of reaction partners based on the same Skyrme energy density functional. Of course, the different density distributions obtained by different approaches will influence the entrance-channel potential. While a self-consistent treatment for both density distribution and the entrance-channel potential seems to be more reasonable.

In this work, the Skyrme energy density functional is applied to make a systematic study of fusion reactions. Firstly, we will use the semi-classical expressions of the Skyrme energy density functional to study the energies and the density distributions of a series of nuclei by the restricted density variational (RDV) method [10,11,13,14]. Secondly, with the density distributions obtained, the entrance-channel potentials of a series of fusion reactions are calculated. Then, based on the entrance-channel potential obtained, a parametrization of the empirical barrier distribution is proposed to take into account the multi-dimensional character of real barrier and then apply it to calculate the fusion excitation functions in terms of barrier penetration concept. The paper is organized as follows: In Section 2, the properties of ground state of nuclei and the entrance-channel potential are studied in the framework of the Skyrme energy density functional. In Section 3, an approach to calculate fusion excitation functions is introduced and a large number of calculated results are presented. Finally, the summary and discussion are given in Section 4.

2. The calculations of fusion barrier

The energy density functional theory is widely used in many-body problems. In the framework of the semi-classical extended Thomas–Fermi (ETF) approach together with a Skyrme effective nuclear interaction, the energy density functional can be derived systematically. We take the Skyrme–Hartree–Fock (Skyrme–HF) formalism of the energy density functional [9,10] and based on it we calculate the proton and neutron densities of nuclei by means of restricted density variational method [10,11,13,14]. With the neutron and proton densities determined in this way we calculate the fusion barrier for fusion reaction based on the same energy density functional.

2.1. Skyrme energy density functional

The total binding energy of a nucleus can be expressed as the integral of energy density functional [9,11]

$$E = \int \mathcal{H} d\mathbf{r}. \quad (1)$$

The energy density functional \mathcal{H} includes the kinetic, nuclear interaction and Coulomb interaction energy parts

$$\mathcal{H} = \frac{\hbar^2}{2m} [\tau_p(\mathbf{r}) + \tau_n(\mathbf{r})] + \mathcal{H}_{\text{sky}}(\mathbf{r}) + \mathcal{H}_{\text{coul}}(\mathbf{r}). \quad (2)$$

For the kinetic energy part, the extended Thomas–Fermi (ETF) approach including all terms up to second order in the spatial derivatives (ETF2), is applied as that was done in Ref. [8]. With the effective-mass form factor [15]

$$f_i(\mathbf{r}) = 1 + \frac{2m}{\hbar^2} \left\{ \frac{1}{4} \left[t_1 \left(1 + \frac{x_1}{2} \right) + t_2 \left(1 + \frac{x_2}{2} \right) \right] \rho(\mathbf{r}) + \frac{1}{4} \left[t_2 \left(x_2 + \frac{1}{2} \right) - t_1 \left(x_1 + \frac{1}{2} \right) \right] \rho_i(\mathbf{r}) \right\}, \quad (3)$$

the kinetic energy densities τ for protons ($i = p$) and neutrons ($i = n$) are given by

$$\tau_i(\mathbf{r}) = \frac{3}{5} (3\pi^2)^{2/3} \rho_i^{5/3} + \frac{1}{36} \frac{(\nabla \rho_i)^2}{\rho_i} + \frac{1}{3} \Delta \rho_i + \frac{1}{6} \frac{\nabla \rho_i \nabla f_i + \rho_i \Delta f_i}{f_i} - \frac{1}{12} \rho_i \left(\frac{\nabla f_i}{f_i} \right)^2 + \frac{1}{2} \rho_i \left(\frac{2m W_0}{\hbar^2} \frac{\nabla(\rho + \rho_i)}{f_i} \right)^2, \quad (4)$$

where ρ_i denotes the proton or neutron density of the nucleus and $\rho = \rho_p + \rho_n$, W_0 denotes the strength of the Skyrme spin–orbit interaction. The nuclear interaction part with Skyrme interaction \mathcal{H}_{sky} reads

$$\begin{aligned} \mathcal{H}_{\text{sky}}(\mathbf{r}) = & \frac{t_0}{2} \left[\left(1 + \frac{1}{2} x_0 \right) \rho^2 - \left(x_0 + \frac{1}{2} \right) (\rho_p^2 + \rho_n^2) \right] \\ & + \frac{1}{12} t_3 \rho^\alpha \left[\left(1 + \frac{1}{2} x_3 \right) \rho^2 - \left(x_3 + \frac{1}{2} \right) (\rho_p^2 + \rho_n^2) \right] \\ & + \frac{1}{4} \left[t_1 \left(1 + \frac{1}{2} x_1 \right) + t_2 \left(1 + \frac{1}{2} x_2 \right) \right] \tau \rho \end{aligned}$$

$$\begin{aligned}
& + \frac{1}{4} \left[t_2 \left(x_2 + \frac{1}{2} \right) - t_1 \left(x_1 + \frac{1}{2} \right) \right] (\tau_p \rho_p + \tau_n \rho_n) \\
& + \frac{1}{16} \left[3t_1 \left(1 + \frac{1}{2} x_1 \right) - t_2 \left(1 + \frac{1}{2} x_2 \right) \right] (\nabla \rho)^2 \\
& - \frac{1}{16} \left[3t_1 \left(x_1 + \frac{1}{2} \right) + t_2 \left(x_2 + \frac{1}{2} \right) \right] [(\nabla \rho_n)^2 + (\nabla \rho_p)^2] \\
& - \frac{W_0^2}{4} \frac{2m}{\hbar^2} \left[\frac{\rho_p}{f_p} (2\nabla \rho_p + \nabla \rho_n)^2 + \frac{\rho_n}{f_n} (2\nabla \rho_n + \nabla \rho_p)^2 \right], \tag{5}
\end{aligned}$$

where $t_0, t_1, t_2, t_3, x_0, x_1, x_2, x_3$, and α are Skyrme-force parameters [8,11]. The last term in the right hand of expression (5) is the semi-classical expansions (up to second order in \hbar) of spin-orbit densities [9]. The Coulomb energy density can be written as the sum of the direct and exchange contribution, the latter being taken into account in the Slater approximation,

$$\mathcal{H}_{\text{Coul}}(\mathbf{r}) = \frac{e^2}{2} \rho_p(\mathbf{r}) \int \frac{\rho_p(\mathbf{r}')}{|\mathbf{r} - \mathbf{r}'|} d\mathbf{r}' - \frac{3e^2}{4} \left(\frac{3}{\pi} \right)^{1/3} (\rho_p(\mathbf{r}))^{4/3}. \tag{6}$$

From the above expressions (1)–(6), one can see that the total energy of a nuclear system can be expressed as a functional of protons and neutrons densities $[\rho_p(\mathbf{r}), \rho_n(\mathbf{r})]$ under the Skyrme interaction associated with the ETF approximation.

2.2. The neutron and proton densities of nuclei

By minimizing the total energy of the system given by expression (1), the neutron and proton densities can be obtained, that is to solve the variational equation

$$\frac{\delta}{\delta \rho_i} \int \{ \mathcal{H}[\rho_n(\mathbf{r}), \rho_p(\mathbf{r})] - \lambda_n \rho_n(\mathbf{r}) - \lambda_p \rho_p(\mathbf{r}) \} d\mathbf{r} = 0, \tag{7}$$

with the Lagrange multipliers λ_n and λ_p to ensure the conservation of neutron and proton number. This density variational problem has been solved in two different ways in the past: either by resolving the Euler–Lagrange equation [13,14] resulting from Eq. (7) or by carrying out the variational calculation in a restricted subspace of functions [10,11,13,14]. In this work we take the neutron and proton density distributions of a nucleus as spherical symmetric Fermi functions

$$\rho_i(\mathbf{r}) = \rho_{0i} \left[1 + \exp\left(\frac{r - R_{0i}}{a_i} \right) \right]^{-1}, \quad i = \{n, p\}. \tag{8}$$

For the three quantities ρ_{0i} , R_{0i} and a_i in the equation, only two of them are independent because of the conservation of particle number $N_i = \int \rho_i(\mathbf{r}) d\mathbf{r}$, $N_i = \{N, Z\}$. For example, ρ_{0p} can be expressed as a function of R_{0p} and a_p ,

$$\rho_{0p} \simeq Z \left\{ \frac{4}{3} \pi R_{0p}^3 \left[1 + \pi^2 \left(\frac{a_p}{R_{0p}} \right)^2 \right] \right\}^{-1} \tag{9}$$

with high accuracy [16] when $R_{0p} \gg a_p$. Here, R_{0p} , a_p , R_{0n} , a_n are the radius and diffuseness for proton and neutron density distributions, respectively.

By using optimization algorithm, one can obtain the minimal energy E_b as well as the corresponding R_{0p} , a_p , R_{0n} , a_n for the neutron and proton density distributions.

The Skyrme force SkM* [17] is adopted in the calculations since SkM* is very successful for describing the bulk properties and surface properties of nuclei. It is a well known fact that

ETF calculations with a reasonable effective interaction reproduce experimental binding energies with a very good accuracy, when Strutinski-type shell corrections and pairing corrections are taken into account. And the obtained charge root-mean-square radii in this work for shell closed nuclei are very close to the corresponding experimental data [18,19]. In addition we have made a comparison between the results with RDV method and the Skyrme–HF method and find that the surface diffuseness obtained by RDV method are little smaller than that by Skyrme–HF calculations. It is due to the neglect of the higher order term corrections in the extended Thomas–Fermi (ETF) approach [10]. We have made a check that the surface diffuseness calculated with RDV method increases if all terms up to fourth order in the spatial derivatives in ETF energy density functional (ETF4) are taken into account.

2.3. The calculations of fusion barriers

The interaction potential $V_b(R)$ between reaction partners can be written as

$$V_b(R) = E_{\text{tot}}(R) - E_1 - E_2, \quad (10)$$

where R is the center-to-center distance between two nuclei, the $E_{\text{tot}}(R)$ is the total energy of the interacting nuclear system, E_1 and E_2 are the energies of individual nuclei (projectile and target), respectively. The interaction potential $V_b(R)$ is also called entrance-channel potential in Ref. [8] or fusion barrier [20,21], in the following we take the term of fusion barrier. The $E_{\text{tot}}(R)$, E_1 , E_2 are calculated with the same energy-density functional as that is used in the calculations of nuclear densities,

$$E_{\text{tot}}(R) = \int \mathcal{H}[\rho_{1p}(\mathbf{r}) + \rho_{2p}(\mathbf{r} - \mathbf{R}), \rho_{1n}(\mathbf{r}) + \rho_{2n}(\mathbf{r} - \mathbf{R})] d\mathbf{r},$$

$$E_1 = \int \mathcal{H}[\rho_{1p}(\mathbf{r}), \rho_{1n}(\mathbf{r})] d\mathbf{r}, \quad (11)$$

$$E_2 = \int \mathcal{H}[\rho_{2p}(\mathbf{r}), \rho_{2n}(\mathbf{r})] d\mathbf{r}. \quad (12)$$

Here, ρ_{1p} , ρ_{2p} , ρ_{1n} and ρ_{2n} are the frozen proton and neutron densities of the projectile and target, determined in the previous section.

For calculating the nuclear interaction energies and Coulomb energies, multi-dimensional integral [22] is performed. For a certain reaction system, the fusion barrier is calculated in a region from $R = 7$ fm to 20 fm with step of $\Delta R = 0.25$ fm. Fig. 1 shows the fusion barrier for the reaction $^{28}\text{Si} + ^{92}\text{Zr}$. The solid curve denotes the results based on the density distributions obtained by RDV method with ETF2. The dotted curve denotes the proximity potential [23]. The results with the density determined by restricted density variational calculations are very close to those of proximity potential at the region where the densities of two nuclei do not overlap.

The fusion barriers for more than 80 fusion systems ($Z_1 Z_2 > 150$) are calculated based on ETF2. Part of them are listed in Table 1. Table 1 lists the barrier height B_0 , radius R_0 (see Fig. 1) and the curvature $\hbar\omega_0$ of the barrier for a series of reactions. Here the curvature of the barrier, $\hbar\omega_0$, is obtained approximately through fitting the barrier at the region from $R_0 - 1.25$ fm to $R_0 + 1.25$ fm by an inverted parabola. From the table, one can find that the curvature of the fusion barrier increases and the Q -value for complete fusion reaction decreases with the increase of product $Z_1 Z_2$.

For exploring the influence of order \hbar^4 terms [10,11], full fourth order ETF (ETF4) is applied to calculate both the densities and the fusion barriers for reactions $^{28}\text{Si} + ^{28}\text{Si}$, $^{40}\text{Ca} + ^{48}\text{Ca}$,

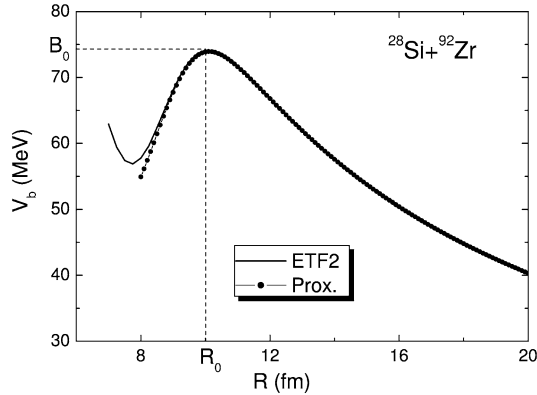
Table 1
The fusion barriers of a series of reactions with ETF2 approach

Reaction	R_0 (fm)	B_0 (MeV)	$\hbar w_0$ (MeV)	$Z_1 Z_2$	Q -value (MeV)	Reference
$^{28}\text{Si} + ^{28}\text{Si}$	8.75	29.86	2.37	196	10.91	[32]
$^{12}\text{C} + ^{92}\text{Zr}$	9.75	33.34	2.10	240	0.94	[1]
$^{16}\text{O} + ^{70}\text{Ge}$	9.25	36.52	2.84	256	2.51	[33]
$^{16}\text{O} + ^{72}\text{Ge}$	9.5	36.27	2.37	256	6.30	[33]
$^{16}\text{O} + ^{73}\text{Ge}$	9.5	36.16	2.44	256	8.84	[33]
$^{16}\text{O} + ^{74}\text{Ge}$	9.5	36.08	2.50	256	10.61	[33]
$^{16}\text{O} + ^{76}\text{Ge}$	9.5	35.80	2.63	256	10.51	[33]
$^{12}\text{C} + ^{128}\text{Te}$	10.25	40.98	2.50	312	-0.91	[34]
$^{16}\text{O} + ^{92}\text{Zr}$	9.75	43.88	2.86	320	-3.94	[1]
$^{16}\text{O} + ^{112}\text{Cd}$	10.0	51.12	3.19	384	-9.91	[35]
$^{27}\text{Al} + ^{70}\text{Ge}$	9.75	57.37	3.26	416	-5.17	[38]
$^{27}\text{Al} + ^{72}\text{Ge}$	9.75	57.05	3.39	416	-4.21	[38]
$^{27}\text{Al} + ^{73}\text{Ge}$	9.75	56.87	3.46	416	-2.90	[38]
$^{27}\text{Al} + ^{74}\text{Ge}$	9.75	56.72	3.51	416	-3.21	[38]
$^{27}\text{Al} + ^{76}\text{Ge}$	10.0	56.31	3.01	416	-2.39	[38]
$^{35}\text{Cl} + ^{54}\text{Fe}$	9.5	61.89	3.67	442	-17.77	[36]
$^{16}\text{O} + ^{144}\text{Nd}$	10.5	61.35	3.27	480	-22.43	[39]
$^{12}\text{C} + ^{204}\text{Pb}$	11.0	59.80	3.19	492	-28.40	[44]
$^{16}\text{O} + ^{144}\text{Sm}$	10.5	63.62	3.27	496	-28.55	[2]
$^{17}\text{O} + ^{144}\text{Sm}$	10.5	63.26	3.41	496	-24.43	[2]
$^{16}\text{O} + ^{147}\text{Sm}$	10.5	63.31	3.37	496	-24.65	[40]
$^{16}\text{O} + ^{148}\text{Sm}$	10.5	63.20	3.41	496	-23.09	[2]
$^{16}\text{O} + ^{149}\text{Sm}$	10.5	63.08	3.46	496	-21.71	[40]
$^{16}\text{O} + ^{150}\text{Sm}$	10.5	62.96	3.49	496	-20.21	[40]
$^{16}\text{O} + ^{154}\text{Sm}$	10.75	62.43	3.07	496	-16.43	[2]
$^{16}\text{O} + ^{166}\text{Er}$	10.75	67.83	3.45	544	-25.13	[41]
$^{28}\text{Si} + ^{92}\text{Zr}$	10.0	74.20	3.97	560	-28.12	[1]
$^{16}\text{O} + ^{186}\text{W}$	11.0	72.26	3.52	592	-21.30	[2]
$^{32}\text{S} + ^{89}\text{Y}$	10.25	82.31	3.76	624	-36.58	[42]
$^{33}\text{S} + ^{90}\text{Zr}$	10.25	84.12	3.87	640	-39.76	[43]
$^{33}\text{S} + ^{92}\text{Zr}$	10.25	83.74	3.97	640	-35.51	[43]
$^{16}\text{O} + ^{208}\text{Pb}$	11.25	78.46	3.54	656	-46.49	[3]
$^{35}\text{Cl} + ^{92}\text{Zr}$	10.25	88.61	4.14	680	-39.37	[1]
$^{19}\text{F} + ^{197}\text{Au}$	11.25	85.21	3.69	711	-35.92	[44]
$^{16}\text{O} + ^{232}\text{Th}$	11.5	84.47	3.68	720	-36.53	[45,46]
$^{32}\text{S} + ^{110}\text{Pd}$	10.5	94.00	4.13	736	-35.37	[47]
$^{36}\text{S} + ^{110}\text{Pd}$	10.5	92.85	4.28	736	-38.01	[47]
$^{19}\text{F} + ^{208}\text{Pb}$	11.25	87.44	3.87	738	-50.07	[48]
$^{40}\text{Ca} + ^{90}\text{Zr}$	10.25	103.74	4.31	800	-57.27	[49]
$^{40}\text{Ca} + ^{96}\text{Zr}$	10.5	102.22	4.28	800	-41.13	[49]
$^{50}\text{Ti} + ^{90}\text{Zr}$	10.5	111.16	4.49	880	-64.73	[50]
$^{32}\text{S} + ^{154}\text{Sm}$	11.0	120.22	4.47	992	-60.69	[51]
$^{28}\text{Si} + ^{178}\text{Hf}$	11.25	120.65	4.41	1008	-64.77	[52]
$^{29}\text{Si} + ^{178}\text{Hf}$	11.25	120.31	4.42	1008	-65.70	[52]
$^{30}\text{Si} + ^{186}\text{W}$	11.5	122.14	4.24	1036	-70.22	[44]
$^{31}\text{P} + ^{175}\text{Lu}$	11.25	126.97	4.46	1065	-70.45	[52]
$^{28}\text{Si} + ^{198}\text{Pt}$	11.5	128.04	4.38	1092	-78.75	[53]
$^{32}\text{S} + ^{181}\text{Ta}$	11.25	138.15	4.56	1168	-80.58	[54]

(continued on next page)

Table 1 (continued)

Reaction	R_0 (fm)	B_0 (MeV)	$\hbar\omega_0$ (MeV)	Z_1Z_2	Q -value (MeV)	Reference
$^{32}\text{S} + ^{182}\text{W}$	11.25	140.02	4.52	1184	-84.93	[55]
$^{132}\text{Sn} + ^{64}\text{Ni}$	11.5	162.75	4.61	1400	-111.05	[56]
$^{40}\text{Ca} + ^{208}\text{Pb}$	11.75	186.57	4.62	1640	-136.69	[57]
$^{48}\text{Ca} + ^{208}\text{Pb}$	12.0	183.17	4.43	1640	-153.80	[57]

Fig. 1. The entrance-channel fusion barrier for $^{28}\text{Si} + ^{92}\text{Zr}$.

$^{16}\text{O} + ^{208}\text{Pb}$, and $^{48}\text{Ca} + ^{208}\text{Pb}$. The similar work had been done by Dobrowolski et al. in [21]. We find that when the \hbar^4 terms [10,11] are included in the determination of the neutron and proton densities, the surface diffuseness of densities of nuclei increases and thus the height of fusion barrier calculated is lower (about 1–2 MeV) than those with ETF2. The fusion barriers for these reactions calculated with different approach are shown in Fig. 2. The dotted curves and the solid curves denote the results with ETF2 and ETF4, respectively, and the crossed curves and the dashed curves denote the results of proximity potential and those of the analytical form proposed in [21], respectively. Our calculation results of barriers with ETF4 are very close to the analytical form in [21]. We find that the barriers calculated with ETF2 are more close to the proximity potential for light and medium-heavy systems (for example, $Z_1Z_2 < 680$), while the barrier calculated with ETF4 are more close to those of proximity potential for heavy systems. It implies that including fourth order terms of ETF approach is important in improving the surface diffuseness for heavy nuclei.

Fig. 3 shows the barrier heights B_0 of the selected systems with ETF2 approach and the relative deviations of B_0 from the proximity potentials B_{prox} [23] as function of Z_1Z_2 . The circles and crosses in Fig. 3(a) denote the results of our calculations and those of proximity potential, respectively. Our calculation results for the barriers are quite close to the proximity potential and the relative deviations are less than 2.5% (see Fig. 3(b)) generally. From the figure one can also see that the barrier heights linearly increase with product Z_1Z_2 . The solid line in Fig. 3(a) is a linear function fit of the calculation results, i.e. $B_{\text{fit}} = \frac{e^2Z_1Z_2}{R_{\text{fit}}} + V_0$ with $R_{\text{fit}} = 13.7$ fm and $V_0 = 13.0$ MeV.

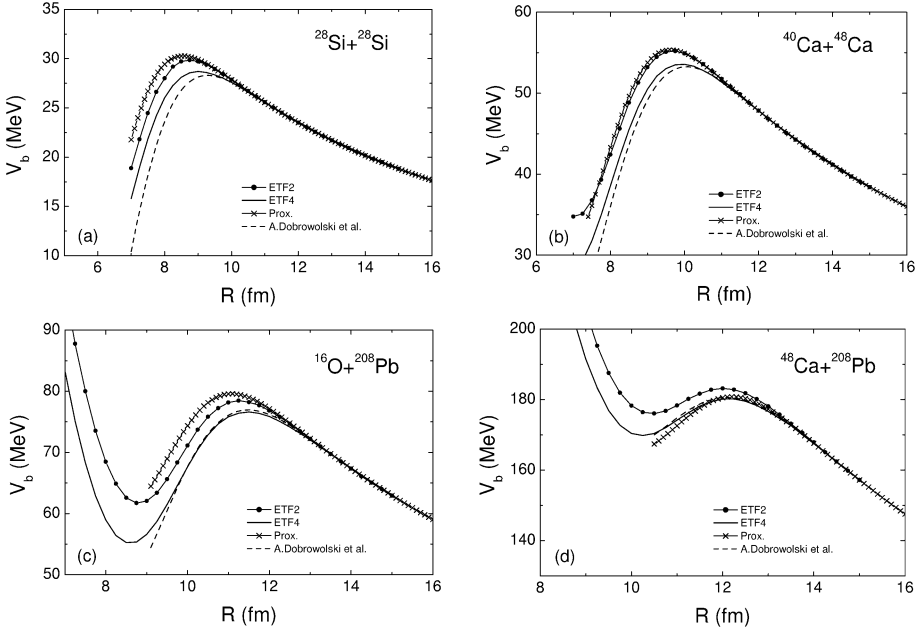


Fig. 2. The fusion barriers for $^{28}\text{Si} + ^{28}\text{Si}$, $^{40}\text{Ca} + ^{46}\text{Ca}$, $^{16}\text{O} + ^{208}\text{Pb}$ and $^{48}\text{Ca} + ^{206}\text{Pb}$. The dotted curves and the solid curves denote the results with ETF2 and ETF4 approach, respectively, and the crossed curves and the dashed curves denotes the results of proximity potential and those of the analytical form proposed in [21], respectively.

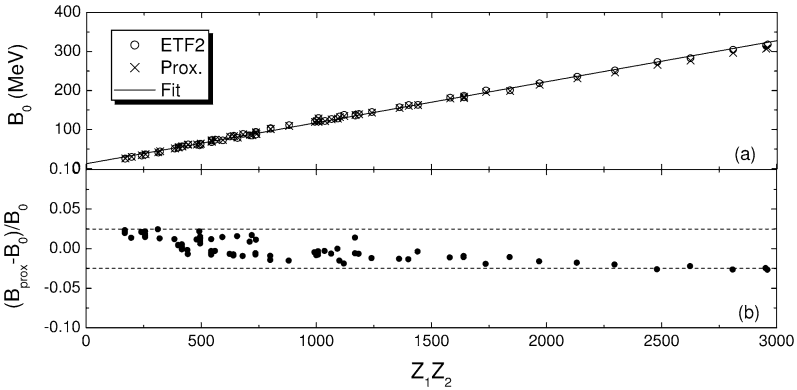


Fig. 3. (a) The barrier heights B_0 for a series of reaction systems and (b) the relative deviations from the results of proximity potential. The circles and crosses in (a) denote the calculation results with RDV and proximity potential, respectively. The solid line is the linearly fitting to our calculations.

3. Fusion excitation functions

3.1. The parametrization of barrier distribution

According to Wong's formula [24], the fusion excitation function for penetrating a parabolic barrier can be expressed as

$$\sigma_{\text{fus}}^{(1)}(E_{\text{c.m.}}, B_0) = \frac{\hbar\omega_0 R_0^2}{2E_{\text{c.m.}}} \ln\left(1 + \exp\left[\frac{2\pi}{\hbar\omega_0}(E_{\text{c.m.}} - B_0)\right]\right), \quad (13)$$

where $E_{c.m.}$ denotes the center-of-mass energy, B_0 , R_0 and $\hbar\omega_0$ are the barrier height, radius and curvature, respectively. This expression is based on the one-dimensional barrier penetration model. The one-dimensional barrier penetration model with empirically determined potential parameters is successful in describing the fusion excitation functions for light systems and heavy systems at energies above the barrier with some exceptions, but fails in describing sub-barrier fusion for heavy systems. It is found that for sub-barrier fusion of heavy systems, the measured fusion cross sections are of up to several orders of magnitude higher than the predictions of the model.

Taking into account the multi-dimensional character [7] of the realistic barrier we may introduce the barrier distribution in order to calculate the total fusion cross sections. Then, the fusion excitation function in terms of barrier penetration concept is given by

$$\sigma_{\text{fus}}(E_{c.m.}) = \int_0^{\infty} D(B) \sigma_{\text{fus}}^{(1)}(E_{c.m.}, B) dB, \quad (14)$$

where $\sigma_{\text{fus}}^{(1)}(E_{c.m.}, B)$ is the fusion excitation function for the barrier B based on one-dimensional barrier penetration, $D(B)$ is a weighing function to describe the barrier distribution. Here we replace the barrier height B_0 in Wong's formula Eq. (13) by B . The distribution function $D(B)$ satisfies

$$\int_0^{\infty} D(B) dB = 1. \quad (15)$$

$D(B)$ is often taken to be continuous and symmetric distributions of rectangular or Gaussian shapes [25–27]. The Wong's formula is a special case when a delta distribution ($D(B) = \delta(B - B_0)$) is taken.

In this work, we propose a parametrization of the weighing function based on the fusion barrier obtained in the previous section. That is that we try to propose a macroscopic empirical barrier distribution rather than explicitly taking into account the coupling of the fusion motion to internal degrees of freedom as that is done in the fusion coupled channel model [28]. Concerning the weighing functions, we first investigate the shape of barrier distributions extracted from experiments. We find in most cases the barrier distributions are not symmetric. For example, in Fig. 4 solid circles show the experimental fusion barrier distribution of $^{16}\text{O} + ^{92}\text{Zr}$ [30]. One can see that the fusion barrier distribution of the reaction system is asymmetric, its left side is steeper than the right side. It indicates that only one Gaussian distribution is not good enough to describe the fusion barrier distribution. Motivated by the shape of the barrier distribution extracted from experiments, we consider the weighing function to be a superposition of two Gaussian functions. Two Gaussian distributions $D_1(B)$ and $D_2(B)$ are proposed as

$$D_1(B) = \frac{\sqrt{\gamma}}{2\sqrt{\pi}w_1} \exp\left[-\gamma \frac{(B - B_1)^2}{(2w_1)^2}\right] \quad (16)$$

and

$$D_2(B) = \frac{1}{2\sqrt{\pi}w_2} \exp\left[-\frac{(B - B_2)^2}{(2w_2)^2}\right], \quad (17)$$

with

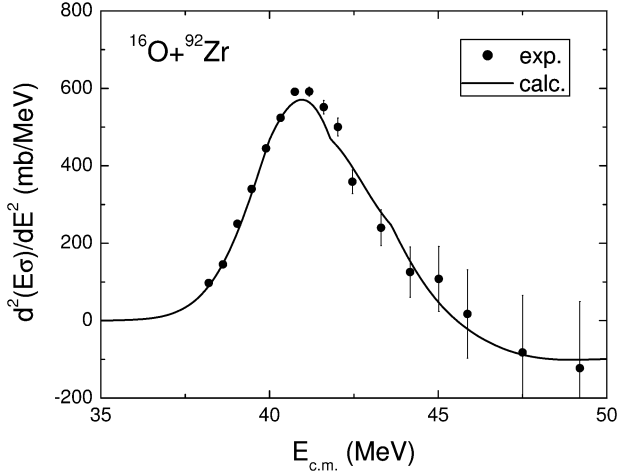


Fig. 4. The fusion barrier distribution for $^{16}\text{O} + ^{92}\text{Zr}$. The distribution is evaluated with $\Delta E_{\text{c.m.}} = 1.8$ MeV. The solid dots and solid curve denote the experimental data and our calculation results, respectively.

$$w_1 = \frac{1}{4}(B_0 - B_c), \quad (18)$$

$$w_2 = \frac{1}{2}(B_0 - B_c), \quad (19)$$

$$B_1 = B_c + w_1, \quad (20)$$

$$B_2 = B_c + w_2. \quad (21)$$

The barrier height B_0 , radius R_0 and curvature $\hbar\omega_0$ are obtained from Table 1. The $B_c = fB_0$ is the effective barrier height taking into account the coupling effects to other degrees of freedom, such as dynamical deformation, nucleon transfer, etc. We take the reducing factor $f = 0.926$. The γ in $D_1(B)$ is a factor which influence the width of the distribution $D_1(B)$. The larger the γ value is, the narrower the distribution is. For the fusion reactions between nuclei with non-closed-shell but near the β -stability line, we take $\gamma = 1$; for the reactions with neutron closed-shell nuclei or neutron-rich nuclei the value of γ is calculated by a parameterized formula which will be discussed in the following subsection. From the expression of (16) and (17) one can find that the peaks and the widths of $D_1(B)$ and $D_2(B)$ only depend on the height of the fusion barrier B_0 except the γ in $D_1(B)$. The peaks of two Gaussian distributions locate at different energies between B_c and B_0 . For light systems, the width of the distribution becomes very small and thus it is very close to delta distribution, in consistent with the one-dimensional penetration model. Both $D_1(B)$ and $D_2(B)$ satisfy Eq. (15). Further we introduce $D_{\text{avr}}(B) = (D_1(B) + D_2(B))/2$. $D_{\text{avr}}(B)$ also satisfies Eq. (15). In Fig. 5 we show the parameterized weighing function of $^{16}\text{O} + ^{186}\text{W}$. The dashed and dot-dashed curves denote Gaussian distributions $D_1(B)$ and $D_2(B)$, respectively. The solid curve denotes the $D_{\text{avr}}(B)$. There are two crossing points between $D_1(B)$ and $D_2(B)$ (or $D_{\text{avr}}(B)$) at both sides of $D_{\text{avr}}(B)$. The left one is located at B_x (see Fig. 5). We notice that the left side of $D_{\text{avr}}(B)$ is too flat and does not fit the shape of the barrier distribution extracted from experimental data well (for example, see the shape shown in Fig. 4). So we propose an effective weighing function

$$D_{\text{eff}}(B) = \begin{cases} D_1(B): & B < B_x, \\ D_{\text{avr}}(B): & B \geq B_x \end{cases} \quad (22)$$

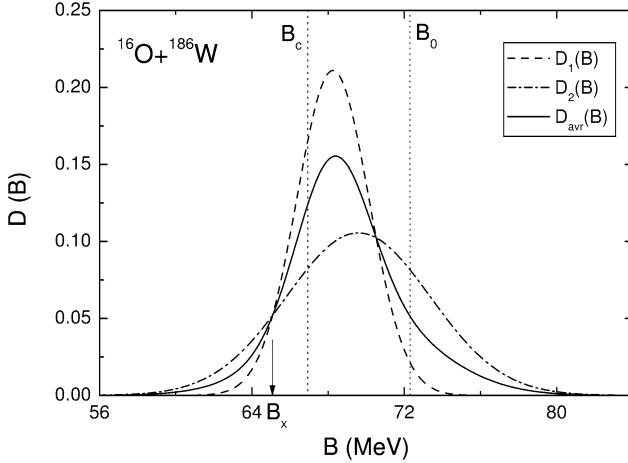


Fig. 5. The weighing function for the fusion reaction of $^{16}\text{O} + ^{186}\text{W}$. The dashed and dot-dashed curves denote Gaussian distributions $D_1(B)$ and $D_2(B)$, respectively. The solid curve denotes the average value, i.e. $D_{\text{avr}}(B) = [D_1(B) + D_2(B)]/2$. The vertical dotted lines denote the positions of B_0 and B_c , respectively. The arrow B_x denotes the cross point between the curves $D_1(B)$ and $D_2(B)$ at the left side of the peak of $D_{\text{avr}}(B)$.

(with $\int D_{\text{eff}}(B) dB \approx 1$). We notice that the distribution $D_1(B)$ plays a main role for sub-barrier fusion and $D_{\text{avr}}(B)$ contributes more to the fusion at energies near and above the barrier.

With the $D_{\text{eff}}(B)$ we can, in principle, calculate the fusion cross sections by the expression

$$\sigma_{\text{fus}}(E_{\text{c.m.}}) = \int_0^{\infty} D_{\text{eff}}(B) \sigma_{\text{fus}}^{(1)}(E_{\text{c.m.}}, B) dB. \quad (23)$$

However, the $D_{\text{eff}}(B)$ does not satisfy Eq. (15) exactly because there is a small difference between $D_1(B)$ and $D_{\text{avr}}(B)$ in the left side of the B_x (see Fig. 5). To remedy this defect, we replace the expression (23) by the following expression in the calculation of fusion cross sections

$$\sigma_{\text{fus}}(E_{\text{c.m.}}) = \min[\sigma_1(E_{\text{c.m.}}), \sigma_{\text{avr}}(E_{\text{c.m.}})]. \quad (24)$$

Here the $\sigma_1(E_{\text{c.m.}})$ and $\sigma_{\text{avr}}(E_{\text{c.m.}})$ are calculated by expression (14) with $D(B) = D_1(B)$ and $D(B) = D_{\text{avr}}(B)$, respectively. Now the normalization condition Eq. (15) is always satisfied for the weighing function adopted in the calculations of fusion cross sections at each $E_{\text{c.m.}}$. We have checked that the fusion cross sections calculated with the expression (24) are very close to those calculated with the expression (23) when the γ is not too large. In fact, we find that the results calculated with Eq. (24) is in better agreement with experimental data. To check the barrier distribution obtained with our model, we also show the barrier distribution obtained from the calculation in Fig. 4 by the solid curve. The good agreement between experimental data and calculation results indicates the parametrization of the weighing function is quite reasonable.

3.2. Fusion reactions between nuclei with non-closed-shell but near β -stability line

In this subsection, the fusion excitation functions for about 30 reaction systems are investigated. For these reaction systems, the projectile and target nuclei are non-closed-shell but near the β -stability line (the shell-closure effects of ^{16}O are neglected in this work). The shell effect and excess neutron effect are weak for this kind reaction systems. Fig. 6 shows the fusion excitation functions of $^{16}\text{O} + ^{186}\text{W}$ and $^{28}\text{Si} + ^{92}\text{Zr}$. From the figure one can find that at energies

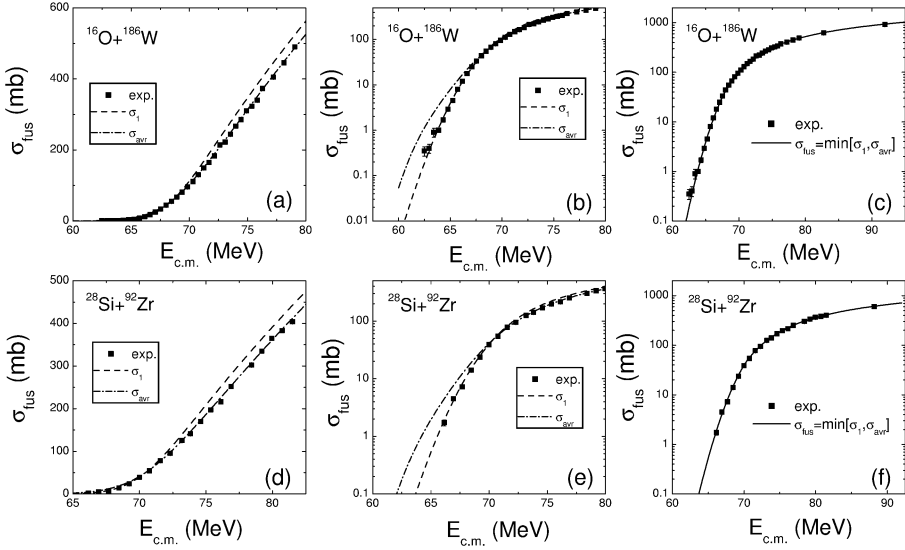


Fig. 6. The fusion excitation functions for $^{16}\text{O} + ^{186}\text{W}$ and $^{28}\text{Si} + ^{92}\text{Zr}$. The dashed and the dot-dashed curves denote the cross sections $\sigma_1(E_{c.m.})$ and $\sigma_{avr}(E_{c.m.})$ calculated with $D(B) = D_1(B)$ and $D(B) = D_{avr}(B)$, respectively.

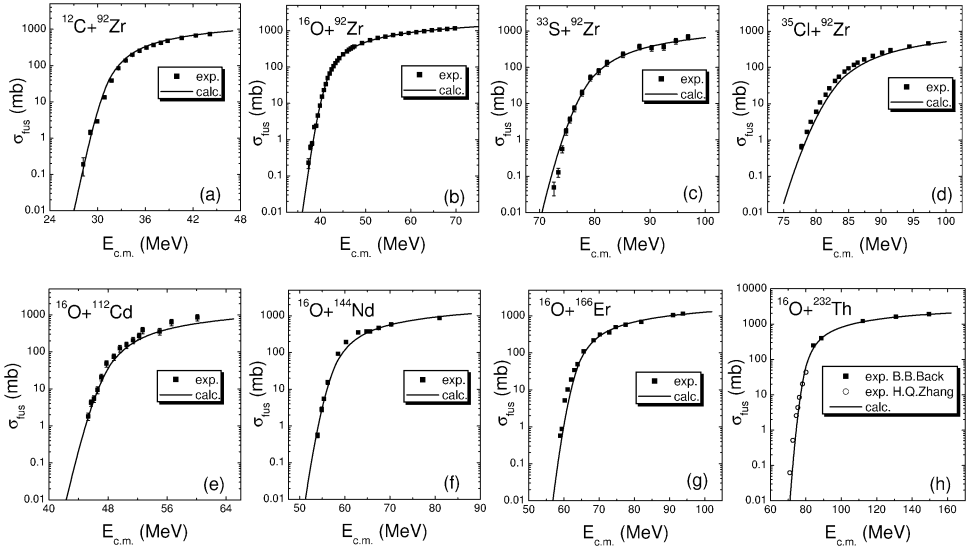


Fig. 7. The fusion excitation functions for ^{12}C , ^{16}O , ^{33}S , $^{35}\text{Cl} + ^{92}\text{Zr}$ and $^{16}\text{O} + ^{112}\text{Cd}$, ^{144}Nd , ^{166}Er , ^{232}Th . The squares denote the experimental data and the solid curves denote the calculation results with $\gamma = 1$.

above the barrier σ_{avr} (dot-dashed curves) is more close to the experimental data, while at energies below the barrier, σ_1 (dashed curves) is preferable. From Fig. 6(c) and (f) one can see that all experimental data spanning the fusion barrier for both $^{16}\text{O} + ^{186}\text{W}$ and $^{28}\text{Si} + ^{92}\text{Zr}$ can be reproduced well. Fig. 7 to Fig. 9 show more calculation results and experimental data for comparison for this kind fusion reactions. All the fusion excitation functions can be reproduced very well, which indicates our parametrization of $D_1(B)$ and $D_2(B)$ is quite useful and reasonable.

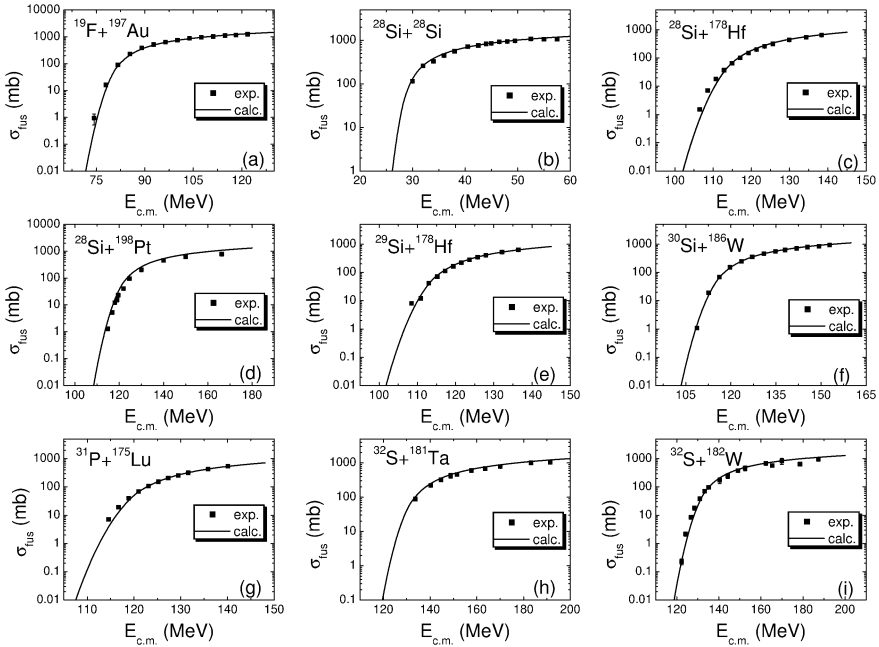


Fig. 8. The fusion excitation functions for $^{19}\text{F} + ^{197}\text{Au}$, $^{28}\text{Si} + ^{28}\text{Si}$, $^{28,29}\text{Si} + ^{178}\text{Hf}$, $^{28}\text{Si} + ^{198}\text{Pt}$, $^{28}\text{Si} + ^{186}\text{W}$, $^{31}\text{P} + ^{175}\text{Lu}$, $^{32}\text{S} + ^{181}\text{Ta}$ and $^{32}\text{S} + ^{182}\text{W}$. The squares denote the experimental data and the solid curves denote the calculation results with $\gamma = 1$.

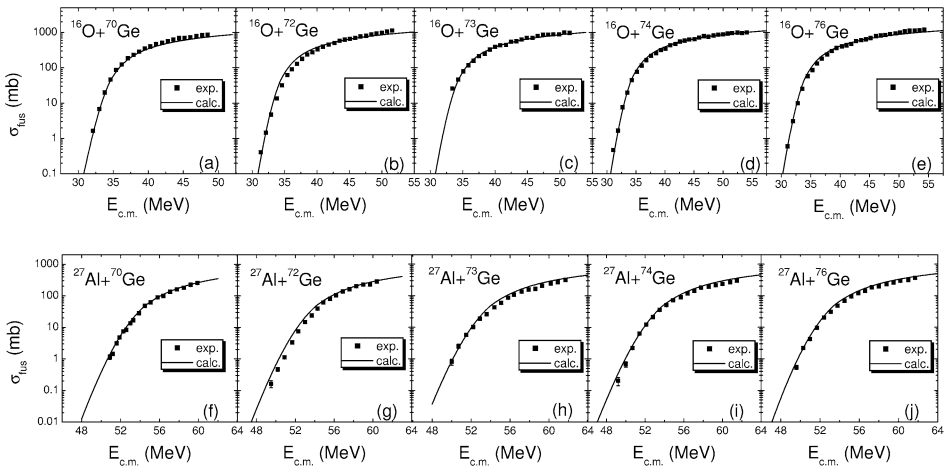


Fig. 9. The fusion excitation functions for ^{16}O , $^{27}\text{Al} + ^{70,72,73,74,76}\text{Ge}$. The squares denote the experimental data and the solid curves denote the calculation results with $\gamma = 1$.

3.3. Fusion reactions between nuclei with neutron-shell-closure or neutron-rich nuclei

The shell effect for neutron closed-shell nuclei and the excess neutron effect for neutron-rich nuclei play an important role in the fusion reactions at energies below the fusion barrier. Fig. 10(a) shows the fusion excitation function of $^{33}\text{S} + ^{90}\text{Zr}$. The dashed curve denotes the

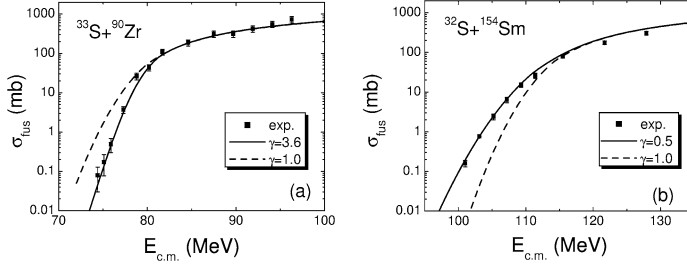


Fig. 10. The fusion excitation functions for reactions $^{33}\text{S} + ^{90}\text{Zr}$, $^{32}\text{S} + ^{154}\text{Sm}$. The squares denote the experimental data. The solid and dashed curves denote the calculation results with the γ values obtained by formula (25) and with $\gamma = 1$, respectively.

calculation results with $\gamma = 1$ and the squares denote the experimental data. One can find that at the energies near and above the barrier B_0 the calculation results with $\gamma = 1$ are in good agreement with the experimental data. However, at sub-barrier energies the fusion cross sections are over-predicted with $\gamma = 1$. Through adjusting the γ value, we find that the fusion excitation function at sub-barrier energies for $^{33}\text{S} + ^{90}\text{Zr}$ can be reproduced reasonably well when $\gamma = 3.6$. Fig. 10(b) shows the fusion excitation function of the neutron-rich nuclear fusion reaction $^{32}\text{S} + ^{154}\text{Sm}$. For this reaction, the fusion cross sections at sub-barrier energies are under-predicted when $\gamma = 1$. For this case, a small γ should be taken so that the distribution $D_1(B)$ is broaden and thus the fusion cross sections are enhanced at sub-barrier energies. We find that when $\gamma = 0.5$ the sub-barrier fusion cross sections can be reproduced well (see Fig. 10(b)). Through systematically analyzing the fusion excitation functions of reactions between nuclei with neutron closed-shell but near the β -stability line and those with neutron-rich nuclei, we find that fusion cross sections are suppressed for the former cases and enhanced for the latter cases compared to the calculation results with $\gamma = 1$. The enhancement of fusion cross sections for reactions with neutron-rich nuclei compared with non-neutron-rich nuclei has been found in Refs. [7,29,30]. It is attributed to the neutron transfer and neck formation which lower the fusion barrier and thus enhance the fusion cross sections at sub-barrier energies [7,29]. For neutron closed-shell nuclei, the strong shell effect suppresses the lowering barrier effect. Based on above discussion we propose an empirical formula for the γ values used in the weighing function $D_1(B)$ for systems with the same Z_1 and Z_2 ,

$$\gamma = 1 - c_0 \Delta Q + 0.5(\delta_n^{\text{prog}} + \delta_n^{\text{targ}}), \quad (25)$$

where $\Delta Q = Q - Q_0$ denotes the difference between the Q -value of the system under considering for complete fusion and that of the reference system. The Q_0 is the Q -value of reference system. $c_0 = 0.5 \text{ MeV}^{-1}$ for $\Delta Q < 0$ cases and $c_0 = 0.1 \text{ MeV}^{-1}$ for $\Delta Q > 0$ cases. $\delta_n^{\text{proj(targ)}} = 1$ for neutron closed-shell projectile (target) nucleus and $\delta_n^{\text{proj(targ)}} = 0$ for non-closed cases (the shell-closure effects of ^{16}O are neglected in this work as mentioned in the above subsection). In addition, we introduce a truncation for γ value, i.e. γ should not be smaller than 0.5.

The reference system is chosen to be the reaction system with nuclei along the β -stability line. More precisely, we do it as follows: from the periodic table we find the relative atomic masses of corresponding elements of projectile and target ($M_{\text{a.m.}}^{\text{proj}}$, $M_{\text{a.m.}}^{\text{tag}}$), then the mass numbers for reaction partners of reference system (A_0^{proj} and A_0^{tag}) can be obtained by inequality $A_0^i - 1 < M_{\text{a.m.}}^i \leq A_0^i$. i denotes projectile ($i = \text{proj}$) or target ($i = \text{tag}$) nuclei. For example, for three fusion reactions $^{16}\text{O} + ^{90,92,96}\text{Zr}$, $^{16}\text{O} + ^{92}\text{Zr}$ reaction system is taken to be the reference system

Table 2

The ΔQ and γ values for a series reactions with neutron closed-shell nuclei or neutron-rich nuclei

Reaction	ΔQ (MeV)	γ	Reference
$^{33}\text{S} + ^{90}\text{Zr}$	-4.25	3.6	[43]
$^{50}\text{Ti} + ^{90}\text{Zr}$	-3.25	3.6	[50]
$^{35}\text{Cl} + ^{54}\text{Fe}$	-6.58	4.8	[36]
$^{16}\text{O} + ^{208}\text{Pb}$	0	1.5	[3]
$^{19}\text{F} + ^{208}\text{Pb}$	0	1.5	[44]
$^{17}\text{O} + ^{144}\text{Sm}$	-0.21	1.6	[2]
$^{32}\text{S} + ^{154}\text{Sm}$	9.80	0.5	[51]
$^{32}\text{S} + ^{110}\text{Pd}$	4.13	0.6	[47]
$^{40}\text{Ca} + ^{96}\text{Zr}$	10.00	0.5	[49]
$^{132}\text{Sn} + ^{64}\text{Ni}$	7.50	0.7	[56]
$^{16}\text{O} + ^{144}\text{Sm}$	-3.91	3.5	[2]
$^{16}\text{O} + ^{147}\text{Sm}$	0	1.0	[40]
$^{16}\text{O} + ^{148}\text{Sm}$	1.56	0.8	[2]
$^{16}\text{O} + ^{149}\text{Sm}$	2.94	0.7	[40]
$^{16}\text{O} + ^{150}\text{Sm}$	4.44	0.6	[40]
$^{16}\text{O} + ^{154}\text{Sm}$	8.22	0.5	[2]
$^{16}\text{O} + ^{144}\text{Sm}$	-3.91	3.5	[2]
$^{16}\text{O} + ^{154}\text{Sm}$	8.22	0.5	[2]
$^{28}\text{Si} + ^{58}\text{Ni}$	-6.81	4.4	[58]
$^{28}\text{Si} + ^{64}\text{Ni}$	8.56	0.5	[58]
$^{36}\text{S} + ^{90}\text{Zr}$	-1.25	2.6	[59]
$^{36}\text{S} + ^{96}\text{Zr}$	7.85	0.7	[59]
$^{40}\text{Ca} + ^{90}\text{Zr}$	-6.14	5.1	[49]
$^{40}\text{Ca} + ^{96}\text{Zr}$	10.00	0.5	[49]
$^{32}\text{S} + ^{110}\text{Pd}$	4.13	0.6	[47]
$^{36}\text{S} + ^{110}\text{Pd}$	1.49	1.3	[47]
$^{40}\text{Ca} + ^{48}\text{Ca}$	10.64	0.9	[37]
$^{48}\text{Ca} + ^{48}\text{Ca}$	3.09	1.7	[37]

according to the atomic mass of O and Zr obtained from periodic table and inequality given above. If there exist certain reaction system for which the experimental data of fusion excitation function can be reproduced well by the calculations with $\gamma = 1$, then this reaction system is preferably chosen as the reference system for the series of reactions with the same Z_1 and Z_2 . For example, for the series of reactions of $^{16}\text{O} + \text{Sm}$, the reaction $^{16}\text{O} + ^{147}\text{Sm}$ is taken as the reference system because the experimental data can be reproduced by the calculations with $\gamma = 1$ (see the following discussion). For this kind of reactions, there may exist possibility of more than one such reaction systems for which the experimental data can be described by the calculations with $\gamma = 1$. This situation might be rare and from our investigation we have not encountered. If this situation occurs we prefer to choosing the reference system according to the inequality given above. The γ values for some fusion reactions with neutron closed-shell nuclei or neutron-rich nuclei are calculated by expression (25) and the results are listed in Table 2. For fusion reactions between nuclei with neutron closed-shell and near the β -stability line, the γ values are larger than 1 (see Table 2), which means that the width of the barrier distribution $D_1(B)$ becomes narrow and thus the fusion cross sections of these systems at sub-barrier energies are suppressed compared with the reference system. Fig. 11 shows the fusion excitation functions of these fusion reactions. One can see from the figure that the experimental data are nicely reproduced.

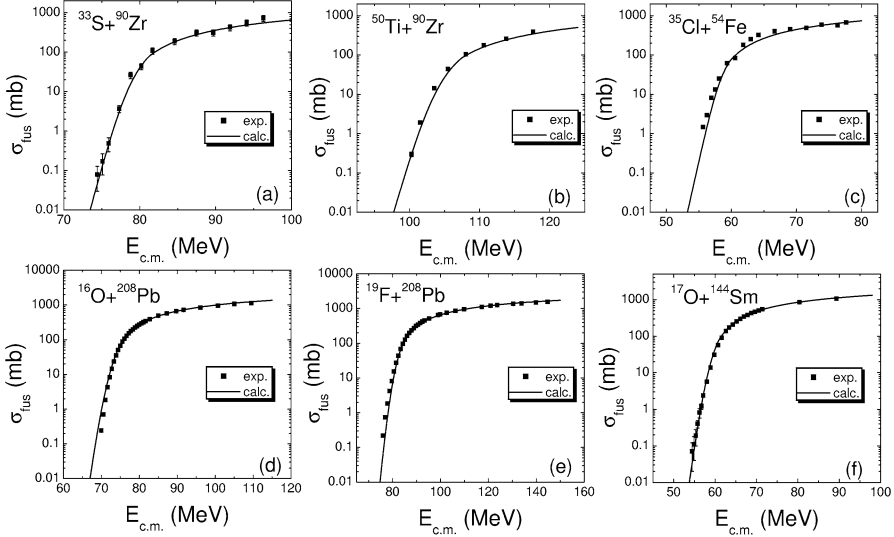


Fig. 11. The fusion excitation functions for reactions $^{33}\text{S} + ^{90}\text{Zr}$, $^{50}\text{Ti} + ^{90}\text{Zr}$, $^{35}\text{Cl} + ^{54}\text{Fe}$, $^{16}\text{O} + ^{208}\text{Pb}$, $^{19}\text{F} + ^{208}\text{Pb}$ and $^{17}\text{O} + ^{144}\text{Sm}$ with neutron-shell-closure nuclei near the β -stability line. The squares denote the experimental data. The solid denote the calculation results with the γ values obtained by formula (25).

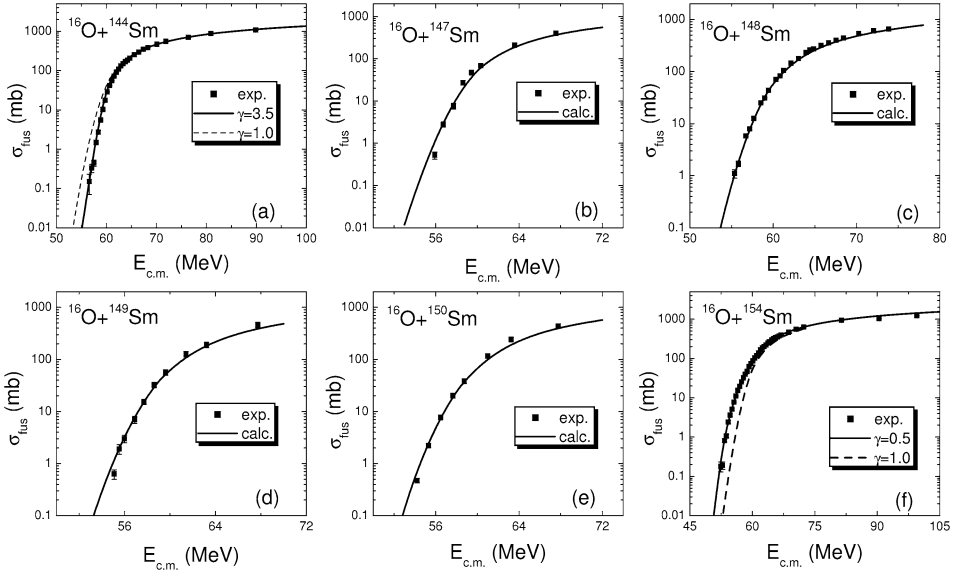


Fig. 12. The fusion excitation functions for $^{16}\text{O} + ^{144,147,148,149,150,154}\text{Sm}$. The squares denote the experimental data. The solid and dashed curves denote the calculation results with γ obtained by formula (25) and with $\gamma = 1$, respectively.

Further, we find that at energies near and above the fusion barrier, calculated fusion cross sections are not sensitive to the value of γ (see Figs. 10 and 12(a), (f)), which implies that we can calculate the fusion cross sections at energies near and above the fusion barrier for unmeasured fusion system by simply taking $\gamma = 1$ in our parametrization of weighing func-

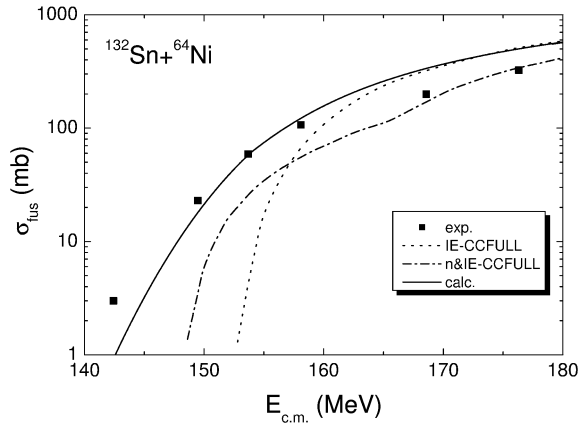


Fig. 13. The fusion excitation functions for $^{132}\text{Sn} + ^{64}\text{Ni}$. The squares denote the experimental data and the solid curves denote the calculated results with γ obtained by formula (25). The dot-dashed and dotted curves denote the results of fusion coupled channel model [31], respectively.

tion. For sub-barrier fusion, more sophisticated investigation for γ value is required. For further investigating the influence of γ value, a series of fusion reactions with ^{16}O projectile on Sm isotope targets from ^{144}Sm to ^{154}Sm are studied. Fig. 12 shows the fusion excitation functions for $^{16}\text{O} + ^{144-154}\text{Sm}$. In the calculations we find that the fusion cross sections for $^{16}\text{O} + ^{147}\text{Sm}$ can be reproduced well by the calculations with $\gamma = 1$ (see Fig. 12(b)), so this system is taken as a reference system for studying other $^{16}\text{O} + ^{144-154}\text{Sm}$. The ΔQ for $^{16}\text{O} + ^{144}\text{Sm}$ is negative as obtained from Table 2 and consequently the corresponding γ value calculated by expression (25) is larger than 1. Thus, this fusion process is unfavored and the fusion cross sections at sub-barrier energies are suppressed compared with reference system $^{16}\text{O} + ^{147}\text{Sm}$. With the increase in numbers of neutrons, the Q -values of reaction under consideration increase gradually and the corresponding γ values decrease, which indicates that the sub-barrier fusion cross sections change from suppression to enhancement compared with the reference system. Our calculated results for O + Sm reactions are in good agreement with the experimental data. For investigating the competition between suppression and enhancement effect of fusion cross sections, six pair reactions of $^{16}\text{O} + ^{144,154}\text{Sm}$, $^{28}\text{Si} + ^{58,64}\text{Ni}$, $^{36}\text{S} + ^{90,96}\text{Zr}$, $^{40}\text{Ca} + ^{90,96}\text{Zr}$, $^{32,36}\text{S} + ^{110}\text{Pd}$ and $^{40,48}\text{Ca} + ^{48}\text{Ca}$ are studied. We find that those reactions with $\gamma < 1$ are all enhanced at sub-barrier energies compared with non-neutron-rich systems, while those reactions with $\gamma > 1$ are all suppressed at sub-barrier fusion compared with neutron non-closed-shell systems.

For radioactive beam fusion reactions $^{132}\text{Sn} + ^{64}\text{Ni}$, the competition exists since ^{132}Sn is both neutron-rich and neutron-shell-closure ($N = 82$, $Z = 50$). The γ value for this reaction is smaller than 1 (see Table 2) and the enhancement of the fusion cross sections at sub-barrier energies is expected. The fusion cross sections of this system are shown in Fig. 13. Squares and solid curve denote the experimental data [56] and our calculation results, respectively. The results of fusion coupled-channel model (the dotted curve denotes inelastic excitations and the dashed curve denotes both the inelastic excitations and neutron transfer are considered [56]) are also presented for comparison. From the comparison one can find that the agreement in sub-barrier fusion cross sections calculated with our approach is better than the fusion coupled channel model [28] calculations. This seems to indicate that there are still some physical aspects missing in present coupled channel calculations.

4. Conclusion and discussion

In this work, the Skyrme energy density functional has been applied to study heavy-ion fusion reactions. The properties of ground state nuclei are studied by using the restricted density variational method with the Skyrme energy density functional plus the semi-classical extended Thomas–Fermi approach (up to second order in \hbar). With the proton and neutron density distributions obtained in this way, the fusion barriers of a series of reaction systems are calculated by the same Skyrme energy density functional. We propose a parametrization for the weighing function describing the empirical barrier distribution based on the fusion barrier calculated with Skyrme energy density functional. The weighing functions of the barrier are assumed to be the superposition of two Gaussian functions. With the parametrization of the weighing function for the empirical barrier distribution, fusion excitation functions for more than 50 systems are calculated. A large number of measured fusion excitation functions spanning the fusion barriers can be reproduced well. The competition between suppression and enhancement effects on sub-barrier fusion caused by neutron-shell-closure and excess neutron effects have been investigated.

However, the proton-shell-closure effects, dynamical effects [29,60] as well as the effects due to large deformation of nuclei in the fusion reactions have not been taken into account in present work, yet. All those effects are very important in fusion dynamics but they are beyond the scope of this work. The study on these aspects is under way.

Acknowledgements

This work is supported by China Postdoctoral Science Foundation, and National Natural Science Foundation of China, Nos. 10235030, 10235020, 10347142, 10375001, Major State Basic Research Development Program under Contract No. G20000774, CAS-grant KJCX2-SW-N02. The website (<http://nr.v.jinr.ru/nrv/webnrv/fusion/reactions.php>), where experimental data for some fusion reactions are accumulated, is acknowledged.

References

- [1] J.O. Newton, C.R. Morton, M. Dasgupta, Phys. Rev. C 64 (2001) 64608.
- [2] J.R. Leigh, M. Dasgupta, D.J. Hinde, Phys. Rev. C 52 (1995) 3151.
- [3] C.R. Morton, A.C. Berriman, M. Dasgupta, Phys. Rev. C 60 (1999) 044608.
- [4] J.O. Newton, R.D. Butt, M. Dasgupta, et al., Phys. Rev. C 70 (2004) 024605.
- [5] V.I. Zagrebaev, et al., Phys. Rev. C 65 (2002) 014607.
- [6] V.I. Zagrebaev, et al., Phys. Rev. C 67 (2003) 061601(R).
- [7] P.H. Stelson, Phys. Lett. B 205 (1988) 190.
- [8] V.Yu. Denisov, W. Noerenberg, Eur. Phys. J. A 15 (2002) 375.
- [9] D. Vautherin, D.M. Brink, Phys. Rev. C 5 (1972) 626.
- [10] M. Brack, C. Guet, H.-B. Hakanson, Phys. Rep. 123 (1985) 275.
- [11] J. Bartel, K. Bencheikh, Eur. Phys. J. A 14 (2002) 179.
- [12] P. Hohenberg, W. Kohn, Phys. Rev. 136 (1964) B864.
- [13] J. Bartel, M. Brack, M. Durand, Nucl. Phys. A 445 (1985) 263.
- [14] M. Centelles, M. Pi, X. Vinas, F. Garcias, M. Barranco, Nucl. Phys. A 510 (1990) 397.
- [15] P. Bonche, H. Flocard, P.H. Heenen, Nucl. Phys. A 467 (1987) 115.
- [16] B. Grammaticos, Z. Phys. A 305 (1982) 257.
- [17] J. Bartel, Ph. Quentin, M. Brack, C. Guet, H.B. Hakansson, Nucl. Phys. A 386 (1982) 79.
- [18] B.A. Brawn, et al., J. Phys. G: Nucl. Phys. 10 (1984) 1683, and references therein.
- [19] G. Fricke, et al., At. Data Nucl. Data Tables 60 (1995) 177.
- [20] R. Bass, Nucl. Phys. A 231 (1974) 45.

- [21] A. Dobrowolski, K. Pomorski, J. Bartel, Nucl. Phys. A 729 (2003) 713.
- [22] J. Berntsen, T.O. Espelid, A. Genz, ACM Trans. Math. Software 17 (4) (1991) 452.
- [23] W.D. Myers, W.J. Swiatecki, Phys. Rev. C 62 (2000) 044610.
- [24] C.Y. Wong, Rev. Lett. 31 (1973) 766.
- [25] H.J. Krappe, et al., Z. Phys. A 314 (1983) 23.
- [26] A.K. Mohanty, S.k. Kataria, Pramana 43 (4) (1994) 319.
- [27] K. Siwek-Wilczynska, J. Wilczynski, Phys. Rev. C 69 (2004) 024611.
- [28] K. Hagino, N. Rowley, A.T. Kruppa, Comput. Phys. Commun. 123 (1999) 143.
- [29] N. Wang, Z. Li, X. Wu, Phys. Rev. C 65 (2002) 064608.
- [30] H. Timmers, D. Ackermann, et al., Nucl. Phys. A 633 (1998) 421, and the doctoral thesis of H. Timmers.
- [31] J.F. Liang, D. Shapira, C.J. Geene, et al., Phys. Rev. Lett. 91 (2003) 152701, and references therein.
- [32] Y. Nagashima, J. Schimizu, T. Nakagava, Phys. Rev. C 33 (1985) 176.
- [33] E.F. Aguilera, J.J. Kolata, R.J. Tighe, Phys. Rev. C 52 (1995) 3101.
- [34] D.E. DiGregorio, Y. Chan, E. Chavez, Phys. Rev. C 43 (1991) 687.
- [35] D. Ackermann, L. Corradi, D.R. Napoli, Nucl. Phys. A 575 (1994) 374.
- [36] E.M. Szanto, R. Liguori Neto, M.C.S. Figueira, Phys. Rev. C 41 (1990) 2164.
- [37] M. Trotta, A.M. Stefanini, L. Corradi, Phys. Rev. C 65 (2001) 011601.
- [38] E.F. Aguilera, J.J. Vega, J.J. Kolata, L. Corradi, Phys. Rev. C 41 (1990) 910.
- [39] G. Duchene, P. Romain, F.A. Beck, Phys. Rev. C 47 (1993) 2043.
- [40] D.E. DiGregorio, M. di Tada, D. Abriola, Phys. Rev. C 39 (1989) 516, and references therein.
- [41] J.O. Fernandez Niello, M. di Tada, A.O. Macchiavelli, Phys. Rev. C 43 (1991) 2303.
- [42] A. Mukherjee, M. Dasgupta, D.J. Hinde, Phys. Rev. C 66 (2002) 34607.
- [43] L. Corradi, S.J. Skorka, U. Lenz, Z. Phys. A 335 (1990) 55.
- [44] D.J. Hinde, A.C. Berriman, R.D. Butt, et al., J. Nucl. Rad. Sci. 3 (1) (2002) 31;
D.J. Hinde, A.C. Berriman, R.D. Butt, et al., Eur. Phys. J. A 13 (2002) 149.
- [45] H. Zhang, J. Xu, Z. Liu, Phys. Rev. C 42 (1990) 1086.
- [46] B.B. Back, R.R. Betts, et al., Phys. Rev. C 32 (1985) 195.
- [47] A.M. Stefanini, D. Ackermann, L. Corradi, Phys. Rev. C 52 (1995) 1727.
- [48] D.J. Hinde, A.C. Berriman, M. Dasgupta, Phys. Rev. C 60 (1999) 054602.
- [49] H. Timmers, D. Ackermann, S. Beghini, L. Corradi, J.H. He, G. Montagnoli, F. Scarlassara, A.M. Stefanini, N. Rowley, Nucl. Phys. A 633 (1998) 421.
- [50] P.H. Stelson, H.J. Kim, M. Beckerman, Phys. Rev. C 41 (1990) 1584.
- [51] P.R.S. Gomes, I.C. Charret, R. Wanis, Phys. Rev. C 49 (1994) 245.
- [52] R.D. Butt, D.J. Hinde, M. Dasgupta, Phys. Rev. C 66 (2002) 44601.
- [53] K. Nishio, H. Ikezoe, S. Mitsuoka, Phys. Rev. C 62 (2000) 014602.
- [54] K.E. Zyromski, W. Loveland, G.A. Souliotis, Phys. Rev. C 63 (2001) 024615.
- [55] S. Mitsuoka, H. Ikezoe, K. Nishio, J. Lu, Phys. Rev. C 62 (2000) 054603.
- [56] J.F. Liang, D. Shapira, C.J. Geene, et al., Phys. Rev. Lett. 91 (2003) 152701, and references therein.
- [57] A.J. Pacheco, J.O. Fernandez Niello, D.E. DiGregorio, Phys. Rev. C 45 (1992) 2861.
- [58] A.M. Stefanini, G. Fortuna, R. Pengo, et al., Nucl. Phys. A 456 (1986) 509.
- [59] A.M. Stefanini, L. Corradi, A.M. Vinodkumar, et al., Phys. Rev. C 62 (2000) 14601.
- [60] N. Wang, Z. Li, X. Wu, et al., Phys. Rev. C 69 (2004) 034608.